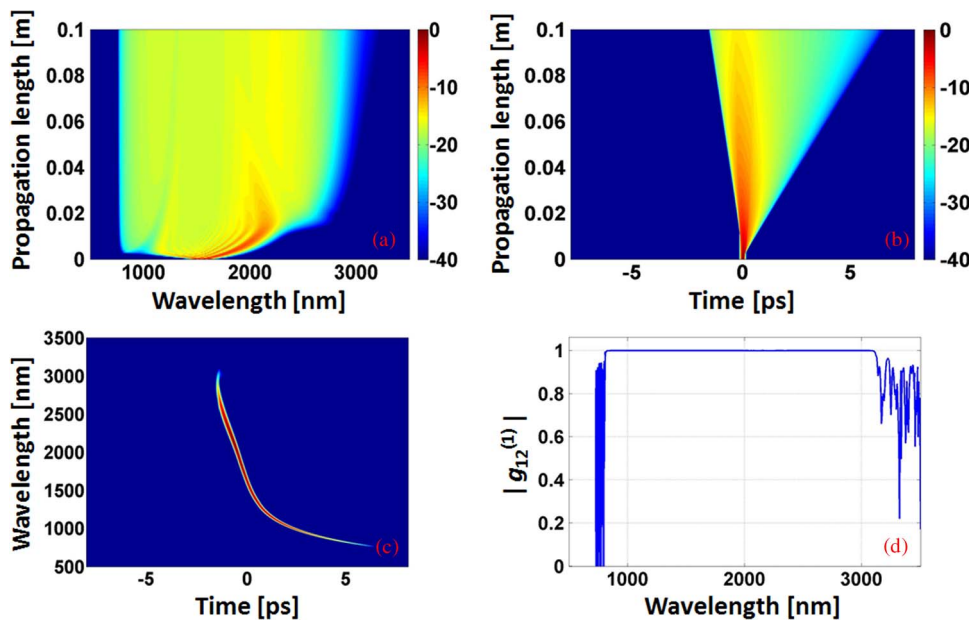


Heavily Germanium-Doped Silica Fiber With a Flat Normal Dispersion Profile

Volume 7, Number 2, April 2015

C. C. Wang
M. H. Wang
J. Wu



Heavily Germanium-Doped Silica Fiber With a Flat Normal Dispersion Profile

C. C. Wang,^{1,2,3} M. H. Wang,^{2,3} and J. Wu^{2,3}

¹Department of Photonics Engineering, Technical University of Denmark,
2800 Kongens Lyngby, Denmark

²Key Laboratory of All Optical Network and Advanced Telecommunication Network of EMC,
Beijing Jiaotong University, Beijing 100044, China

³Institute of Lightwave Technology, Beijing Jiaotong University, Beijing 100044, China

DOI: 10.1109/JPHOT.2015.2409232

1943-0655 © 2015 IEEE. Translations and content mining are permitted for academic research only.
Personal use is also permitted, but republication/redistribution requires IEEE permission.
See http://www.ieee.org/publications_standards/publications/rights/index.html for more information.

Manuscript received January 4, 2015; revised February 25, 2015; accepted February 25, 2015. Date of current version March 17, 2015. This work was supported by the Basic Scientific Research Foundation of Beijing Jiaotong University under Grant 2013JBM012. Corresponding author: C. C. Wang (e-mail: xzwangchuncan@126.com).

Abstract: A heavily germanium-doped (Ge-doped) silica fiber with a four-layer refractive index profile is proposed to obtain all normal flat dispersion property. The waveguide dispersion in the fiber can be modified by adjusting the fiber parameters, including the refractive indices and the core radiiuses. As a result, the flat normal dispersion in the fiber can be obtained in the wavelength range of 1540–2600 nm, where the values of the dispersion slope are between –0.0058 and 0.03 ps/nm²/km. Furthermore, the numerical results show that the flat-top supercontinuum spectrum ranging from 1000 to 2600 nm can be generated by launching pump pulses at the wavelength of 1550 nm in the heavily Ge-doped fiber with a four-layer refractive index profile.

Index Terms: Fiber nonlinear optics, supercontinuum generation, four-wave mixing.

1. Introduction

Supercontinuum (SC) generation in all-normal dispersion fiber (ANDF) has gained much attention due to the perfect coherent properties, which is of particular importance for time-critical applications such as optical coherence tomography [1], nonlinear microscopy [2], and ultra-short pulse generation [3]. Furthermore, the experimental and theoretical results show that the ANDF with a flat dispersion profile is desired to obtain the broadband flat-top SC spectra, which is especially critical for the application in time-resolved measurements [4]. Recently, the coherent SC generation in ANDF were experimentally demonstrated in the visible and near infrared wavelength ranges [5]–[9] and 900–2300 nm [10]. The ANDF with a flattened convex profile of the dispersion can be realized based on the typical photonic crystal fiber (PCF) with the regular triangular air-hole cladding [5], [7]–[9], [11]. The dispersion profile can be further flattened for the PCFs with a triangular hybrid core region [12]; inner air-hole rings in the core area [13], [14]; a square-lattice cladding [15]; or a hybrid cladding [16]. However, the dispersion property of the air-glass PCF is sensitive to the structural distortion because of the large air/glass refractive index difference. For this reason, producing the air-glass PCFs with desired dispersion profiles requires an accurate control of geometric parameters, which is very difficult during the fiber fabrication process, especially for the PCF with a complex structure of air-hole cladding. Recently, it was experimentally demonstrated that all-solid, low index contrast fibers with a tailored

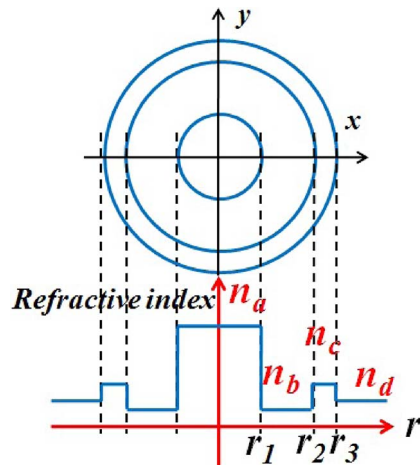


Fig. 1. Cross section of the heavily Ge-doped fiber, where n_a , n_b , n_c , and n_d represent the refractive indices of the cores and cladding with the different germanium concentrations. r_1 , r_2 , and r_3 are the corresponding radii of the cores from inside out.

dispersion profile and high nonlinearity can provide an efficient way to reduce the difficulties in the fiber fabrication process. The all-solid soft glass PCF with a flattened normal dispersion in the wavelength range of $1.5\text{--}2.5 \mu\text{m}$ was used to generate a coherent SC spectrum spanning $900\text{--}2300 \text{ nm}$ [10], [17]. The lead silicate fiber with a W-type index profile exhibits a near zero flat dispersion profile in the $1.55 \mu\text{m}$ region, where the nonlinearity coefficient can be as high as $0.82 \text{ W}^{-1}/\text{m}$ because the nonlinearity refractive index of glass SF57 is higher than that of silica by 20 times [18]. Furthermore, the flat dispersion profile around other desired wavelength region of interest can be obtained by tuning geometric parameters of the fiber and a proper selection of core and cladding glasses [19]. However, the lead silicate W-type fiber is not suitable for coherent SC generation with the spectral width of more than one octave because of the limited wavelength bandwidth of the flat dispersion region.

In this paper, an approach based on the heavily Ge-doped silica fiber with a four-layer refractive index profile as shown in the Fig. 1 is proposed to obtain the flat normal dispersion in the fiber. It has been experimentally demonstrated that the germanium concentration in the silica fiber can be increased from 30% to 100% [20]–[23], which provides an additional degree of freedom for optimizing the waveguide dispersion in the fiber.

2. Theory for the Simulation

The refractive index dispersion for the Ge-doped silica is given by the Sellmeier dispersion equation [24]

$$n^2(\lambda) - 1 = \sum_{i=1}^3 \frac{[SA_i + X(GA_i - SA_i)]\lambda^2}{\lambda^2 - [SI_i + X(GI_i - SI_i)]^2} \quad (1)$$

where n is the refractive index of Ge-doped silica; λ is the wavelength in a vacuum; and SA_i , SI_i , GA_i , and GI_i are the Sellmeier coefficients for the SiO_2 and GeO_2 glasses, respectively. The value of X is the GeO_2 concentration in mol%.

The total dispersion includes the contributions of the material dispersion and waveguide dispersion. Since the material dispersion of the Ge-doped silica is included when solving the wave propagation equation by using the full-vectorial finite element method (FVFEM) solver Comsol, the group velocity dispersion (GVD) can be written as

$$D(\lambda) = -\frac{\lambda}{c} \frac{d^2 n_{FM}(\lambda)}{d\lambda^2} \quad (2)$$

where $n_{\text{FM}}(\lambda)$ is the effective index of the fundamental mode (FM) at the operating wavelength λ . c is the velocity of light in a vacuum. Since the intensity of the FM distributes in the Ge-doped silica areas with the different nonlinearity refractive index (NRI) $n_2(x, y)$, the nonlinearity coefficient $\gamma(\lambda)$ can be defined as [25]

$$\gamma(\lambda) = \frac{2\pi \int \int_{-\infty}^{\infty} n_2(x, y) |\vec{E}_t|^4 dx dy}{\lambda \left(\int \int_{-\infty}^{\infty} |\vec{E}_t|^2 dx dy \right)^2} \quad (3)$$

where $|\vec{E}_t|$ is the magnitude of the electric field vector \vec{E}_t in the x and y directions. The NRI n_2 in the fiber is $(2.16 + 0.033X)$, where the unit is $10^{-20} \text{ m}^2/\text{W}$ [26], [27].

The confinement loss of the modes in the fiber with a four-layer refractive index profile can be defined by

$$L_C = \frac{20}{\ln(10)} \frac{2\pi}{\lambda} \text{Im}(n_{\text{eff}}) \text{ dB/m} \quad (4)$$

where $\text{Im}(n_{\text{eff}})$ represents the imaginary part of the effective index of the modes. Additionally, the absorption loss including Rayleigh scattering and infrared absorption in GeO_2 fiber is given by [23]

$$L_A = 2.3/\lambda^4 + 0.4 \times 10^{11} \exp(-58/\lambda), \quad 1 \times 10^{-3} \text{ dB/m}. \quad (5)$$

Consequently, the total loss L_{total} is the sum of the confinement loss L_C and absorption loss L_A .

The evolution of the pulse envelope in the fiber can be described by the generalized nonlinear Schrödinger equation (GNLSE), which is given by [28]

$$\frac{\partial A}{\partial z} + \frac{\alpha}{2} A - \sum_{k \geq 2} \frac{i^{k+1}}{k!} \beta_k \frac{\partial^k A}{\partial T^k} = i\gamma \left(1 + i\tau_{\text{shock}} \frac{\partial}{\partial T} \right) \times \left[A(z, T) \int_{-\infty}^{+\infty} R(T') |A(z, T - T')|^2 dT' \right] \quad (6)$$

where $A(z, T)$ represents the slowly varying pulse envelope in time domain, T is the retarded time for a comoving frame at the envelope group velocity $1/\beta_1$, α is the linear loss, β_k are the dispersion coefficients associated with the Taylor series expansion of the propagation constant $\beta(\omega)$ around the center frequency ω_0 . In the process of solving GNLS, the dispersion operator in the frequency domain is applied through multiplication of the complex spectral envelope $\tilde{A}(z, \omega)$ by the operator $\beta(\omega) - (\omega - \omega_0)\beta_1 - \beta_0$. The time derivative term on the right-hand side models the dispersion of the nonlinearity, which is associated with the effects of self-steepening and optical shock formation, characterized by a time scale $\tau_{\text{shock}} = 1/\omega_0$. The nonlinear response function $R(T) = (1 - f_R)(\delta T) + f_R hR(T)$ includes both instantaneous and delayed Raman contributions. The fractional contribution of the delayed Raman response to nonlinear polarization f_R is 0.18. In the fiber core with a high GeO_2 concentration, the Raman response term $h_R(t)$ is given by [29]

$$h_R(T) = \frac{\tau_s^2 + \tau_v^2}{\tau_s \tau_v} \exp(-T/\tau_v) \sin(T/\tau_s) \Theta(T) \quad (7)$$

where the time constants τ_s and τ_v are related to the frequency of the “phonon” and the attenuation of the network of vibrating atoms for GeO_2 , respectively. The values of τ_s and τ_v are taken to be 12.2 and 83 fs, respectively. $\Theta(T)$ is Heaviside step function.

In the following simulations, the initial pulse is set to be a Gaussian pulse $A_0(T) = \sqrt{P_0} \exp(-T^2/T_0^2)$, where $T_0 = T_{\text{FWHM}}/\sqrt{2\ln 2}$, and T_{FWHM} is the full width at half-maximum (FWHM) pulse duration. The peak power P_0 can be obtained by $P_0 = 0.94 E_0 / T_{\text{FWHM}}$, where E_0 is the pulse energy.

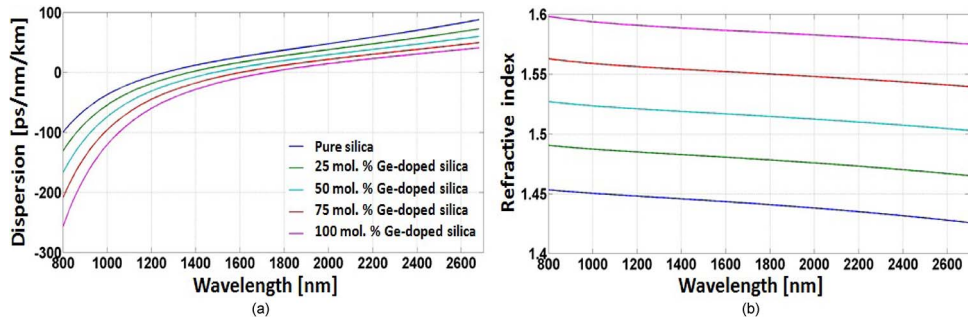


Fig. 2. (a) Curves of the material dispersions and (b) refractive indices for the pure silica and Ge-doped silica with the different germanium concentrations.

3. Numerical Results and Discussions

3.1. Dispersion and Nonlinearity Coefficient

According to the Sellmeier dispersion equation [24], the material dispersion in the Ge-doped silica can be calculated and described in Fig. 2(a). The numerical results show that the zero dispersion wavelength (ZDW) for the heavily Ge-doped silica shifts toward longer wavelength regime with increasing the germanium concentration X . When $X = 100$ mol%, the corresponding ZDW is 1730 nm, which is located 470 nm away from the ZDW of the pure silica [24]. Moreover, it can be seen in Fig. 2(b) that the refractive index difference between the Ge-doped silica and pure silica can reach up to 0.14 over the wavelength ranging from 800 to 2700 nm. Compared with the fiber based on the air-silica structure, the red shift of the ZDW and selectable refractive index difference are helpful to obtain a broad and flat normal dispersion profile within the near infrared regime.

First, the influence of the refractive index distribution on the dispersion is analyzed with the constant geometric parameters as shown in Fig. 3. Assuming $n_a = n(X = 100 \text{ mol}\%)$, one can see that the maximum dispersion shifts toward the normal dispersion regime with increasing the value of n_b in Fig. 3(a). At the same time, the absolute values of the $D(\lambda)$ on the longer wavelength side decrease. As a result, the dispersion profile (red curve) can be flattened in the wavelength range of around 1500–2600 nm. During the process of the SC generation, a low absolute value of the GVD at the maximum dispersion wavelength (MDW) can lead to a depletion of the mid-section spectrum via the effect of four wave mixing (FWM). When increasing the absolute value of the GVD at the MDW, the flat-top SC spectrum can be obtained. However, the wavelength bandwidth of the generated SC spectrum decreases with an increase of the absolute value of the GVD [4]. Consequently, it is necessary to adjust the value of the GVD at the MDW in the fiber for a broadband flat-top SC generation. As shown in Fig. 3(b), the value of $D(\lambda)$ in the wavelength range of 1500–2300 nm can be modified without a degradation of the dispersion flatness by an appropriate choice of the value of n_c . In Fig. 3(c), one can see that increasing the value of n_d can lead to lowering the dispersion profile especially at the longer wavelengths.

Moreover, Fig. 4 shows the influence of the deviation of the geometric parameters on the dispersion profiles in the fiber. It can be seen that when the values of r_1 are changed by $\pm 2\%$ or $\pm 5\%$, the variations of the dispersion curves in both cases are larger than those when the other parameters are changed. The reason is that the intensities of the FMs mostly distribute in the inner core with the radius of r_1 . Furthermore, the variations in the dispersion $D(\lambda)$ induced by the deviations of the radius r_1 in the former case are below 3.24 ps/nm/km, which is lower than 8.55 ps/nm/km corresponding to the latter case. The results imply that the deviations from the desired geometric parameters needs to be carefully controlled within $\pm 2\%$, especially for the radius r_1 .

So far, n_a is set to be $n(X = 100 \text{ mol}\%)$. When the germanium concentration X corresponding to n_a decreases from 100 mol% to 60 mol%, the other parameters including the refractive

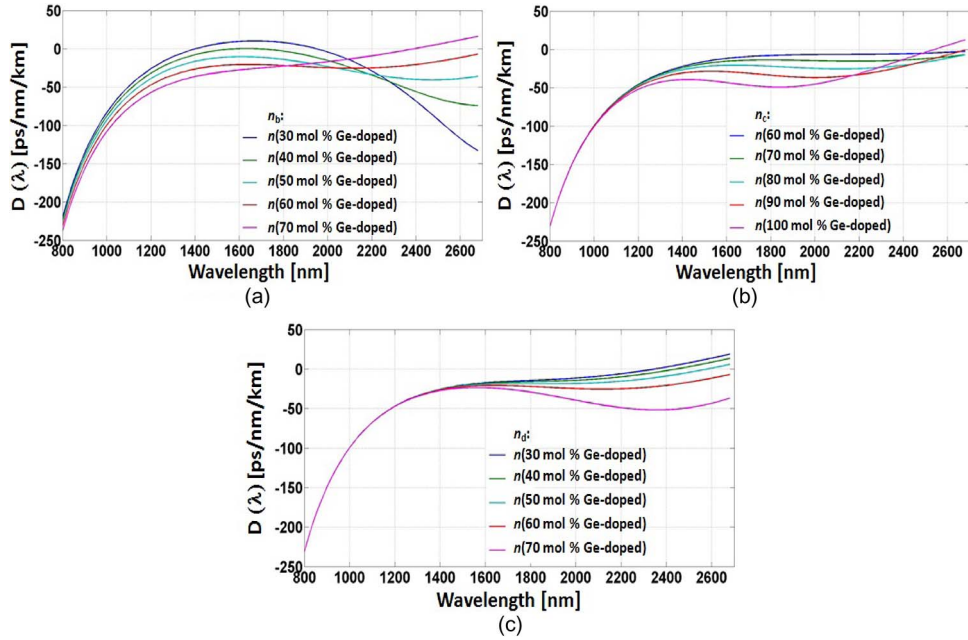


Fig. 3. Dispersion $D(\lambda)$ for the different values of (a) n_b , (b) n_c , or (c) n_d , where $r_1 = 1.7 \mu\text{m}$, $r_2 = 3.3 \mu\text{m}$, $r_3 = 4.3 \mu\text{m}$, and $n_a = n$ ($X = 100 \text{ mol\%}$). The other parameters are (a) $n_c = n$ ($X = 80 \text{ mol\%}$), $n_d = n$ ($X = 60 \text{ mol\%}$); (b) $n_b = n$ ($X = 60 \text{ mol\%}$), $n_d = n$ ($X = 60 \text{ mol\%}$); and (c) $n_b = n$ ($X = 60 \text{ mol\%}$), $n_c = n$ ($X = 80 \text{ mol\%}$).

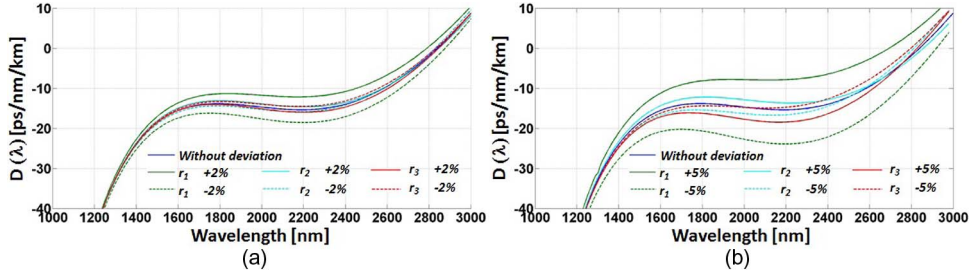


Fig. 4. Dispersion $D(\lambda)$ with and without the deviations of $\pm 2\%$ (a) and $\pm 5\%$ (b) from the parameters r_1 , r_2 , and r_3 . The parameters without the deviations are identical to those of the curve A in Table 1.

indices and core radii are adjusted accordingly so that the values of the GVD at the MDW remain unchanged as shown in Fig. 5(a). One can see that the dispersion profile is blue-shifted with decreasing the value of n_a . The reason can be understood by noting that the ZDW of the material dispersion for the Ge-doped silica shifts toward the blue side with reducing the concentration X as shown in Fig. 2(a). Furthermore, the dispersion slope curves corresponding to the dispersion cures in Fig. 5(a) are presented in Fig. 5(b). For the curve A, the values of the dispersion slope over the spectral range 1540–2600 nm are between -0.0058 and $0.03 \text{ ps/nm}^2/\text{km}$. When decreasing the values of n_a , the wavelength range with the dispersion slope below $0.03 \text{ ps/nm}^2/\text{km}$ decreases and has a blue shift. These results indicate that, the heavily Ge-doped fibers with proper choices of geometric parameters of the fiber and germanium concentrations can exhibit much broader wavelength bandwidth of the flat dispersion region compared with the W-type fibers in [18] and [19]. Both the shape of the dispersion profile and flat dispersion wavelength region are similar to those of the soft-glass PCF in [10]. It implies that the heavily Ge-doped fiber presented here can offer an interesting way to realize coherent SC generation because of the simple fiber structure and broadband range of the flat normal dispersion.

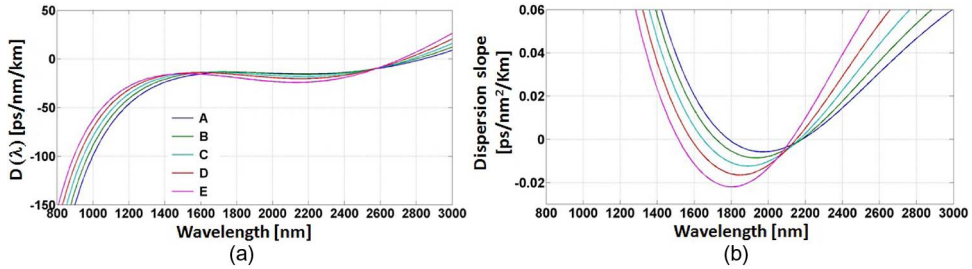


Fig. 5. (a) Curves of the dispersion $D(\lambda)$ and (b) corresponding dispersion slope for the different values of n_a . The fiber parameters are shown in Table 1.

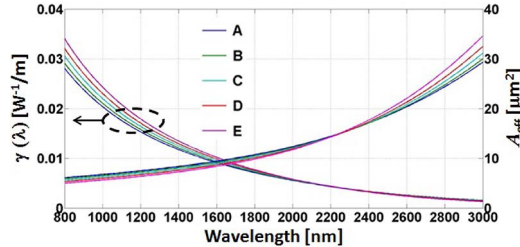


Fig. 6. (Left) Nonlinearity coefficient $\gamma(\lambda)$ and (right) mode effective area A_{eff} for the different values of n_a . The parameters for the five curves are presented in Table 1.

Moreover, as shown in Fig. 6, the mode effective areas A_{eff} of the FM increase with the wavelength. For this reason, the nonlinearity coefficients decrease with increasing the wavelength. When the wavelength is 1550 nm, the nonlinearity coefficients for all the five curves are more than $0.0096 \text{ W}^{-1}/\text{m}$, which is lower than that of the W-type fiber in [18] because of the large A_{eff} of the FM and relatively low nonlinearity refractive index in Ge-doped silica.

3.2. Loss of the Modes in the Fiber

Both the confinement loss and absorption loss are taken into account in Fig. 7. It can be seen that, when the wavelengths are $> 1500 \text{ nm}$, the confinement losses of the first high order modes increase rapidly with wavelengths. For this reason, the total losses of the first high order modes are much higher than those of the FMs. For example, as shown in Fig. 7(a), the values of L_{total} at the wavelength of 1550 nm are 0.0004, 0.15, 0.19, and 0.23 dB/m for the modes HE_{11} , TE_{01} , TM_{01} , and HE_{21} , respectively. In Fig. 7(c), the corresponding values of L_{total} at the wavelength of 1550 nm are 0.0004, 11.7, 13.3, and 18.1 dB/m, respectively. The difference of losses between the FMs and high order modes can be further increased by bending the fiber with a proper bending radius. For this reason, a single-mode operation in the fiber at wavelengths $> 1500 \text{ nm}$ is feasible. When the wavelengths are $< 1300 \text{ nm}$, the absorption losses dominate in the total losses for both the FMs and first high order modes. In this case, the fiber supports a multimode operation at wavelengths $< 1300 \text{ nm}$. However, if only the FM is pumped by a proper input optical field, the dominant nonlinear mechanisms only result in a power transfer from the FM into the high order mode LP_{02} (HE_{21}) at the pump wavelength [30]. For the heavily Ge-doped fiber with the parameters in Table 1, the high order mode LP_{02} (HE_{21}) is cut off at the pump wavelength of 1550 nm. As a result, when only the FM in the fiber is excited at the pump wavelength, the SC can be generated in the FM with negligible power transfer between the FM and high-order modes.

3.3. Flat-Top SC Generation

The spectra and temporal evolution with the propagation distance are shown in Fig. 8(a). It can be seen that in the initial stage the blue side of the self phase modulation (SPM) generated spectrum can extend to around 1200 nm, and then, these high frequency components act as

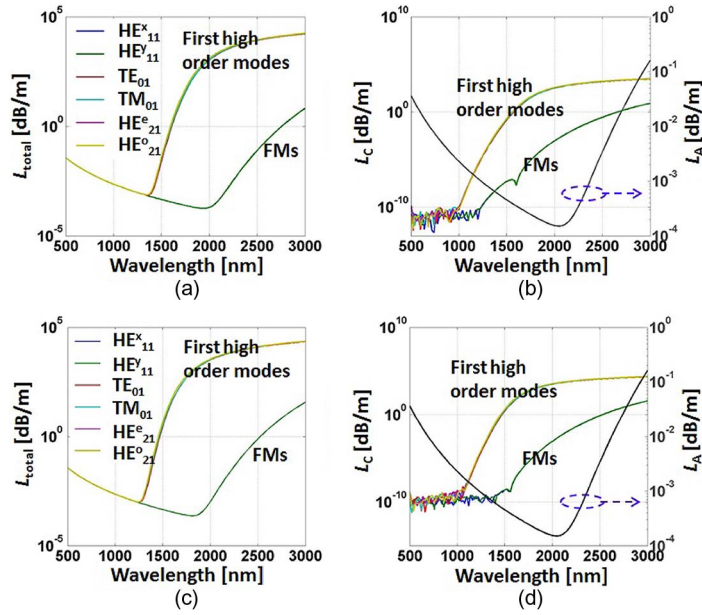


Fig. 7. (a) and (c) Total losses L_{total} and (b) and (d) (left) confinement loss L_C and (right) absorption loss L_A for the fundamental modes (HE_{11}^X and HE_{11}^Y) and the first high order modes (TE_{01} , TM_{01} , HE_{21}^e , and HE_{21}^o) in the fiber. The corresponding parameters in Fig. 7(a)–(b) and (c)–(d) are identical to those of the curves A and D in Table 1, respectively.

TABLE 1

Fiber parameters in Figs. 4 and 5

Curve	n_a : X (mol %)	n_b : X (mol %)	n_c : X (mol %)	n_d : X (mol %)	r_1 (μm)	r_2 (μm)	r_3 (μm)
A	100	60	70	60	1.7	3.3	4.3
B	90	50	60	50	1.66	3.3	4.3
C	80	40	50	40	1.61	3.3	4.3
D	70	30	40	30	1.56	3.3	4.3
E	60	20	30	20	1.50	3.3	4.3

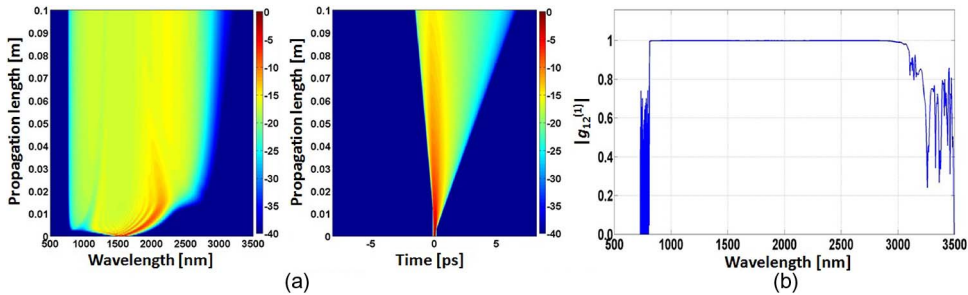


Fig. 8. (Left) Spectral and (right) temporal evolution with (a) the propagation distance (b) and the degree of coherence $|g_{12}^{(1)}(\lambda)|$ of the pulse at the propagation distance of 0.1 m. The central wavelength of the pump pulse is 1550 nm with $E_0 = 25 \text{ nJ}$ and $T_{\text{FWHM}} = 100 \text{ fs}$. The other parameters of the fiber are identical to the curve A in Table 1.

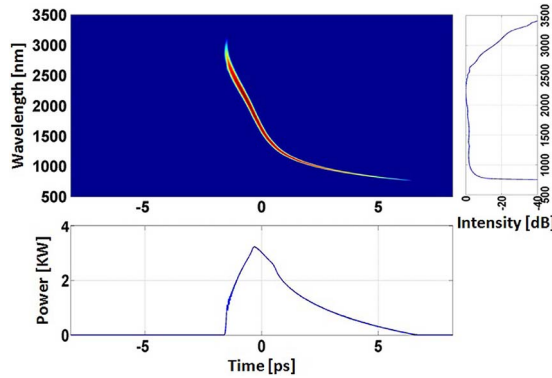


Fig. 9. Calculated spectrogram of the pulse at the propagation distance of 0.1 m. The other parameters are identical to those of Fig. 8.

pumps in the subsequent FWM process. As a result, the spectral sidelobe as the FWM products appears in the vicinity of the wavelength of 1000 nm with further propagation. Additionally, on the long wavelength side the spectrum generated by SPM combined with the effect of the stimulated Raman scattering (SRS) can extend to 2500 nm. For lasing in the 1550 nm window, Er doped or Er/Yb co-doped fiber laser can be a good pump laser source because of their high power handling, large heat dissipation, excellent beam quality, and robustness. Thus, it is interesting to generate the near infrared SC spectra ranging from 1000 to 2500 nm with a flat spectral profile by using a fiber laser as the pump laser source. Moreover, the complex degree of first-order coherence can be defined at each wavelength in the SC by [28]

$$|g_{12}^{(1)}(\lambda, t_1 - t_2)| = \left| \frac{\langle E_1^*(\lambda, t_1) E_2(\lambda, t_2) \rangle}{\sqrt{\langle |E_1(\lambda, t_1)|^2 \rangle \langle |E_2(\lambda, t_2)|^2 \rangle}} \right| \quad (8)$$

where angular brackets denote an ensemble average over independently generated pairs of SC spectra $[E_1(\lambda, t), E_2(\lambda, t)]$ obtained from 60 independently simulations. The random quantum noise is added into the input pulse with one photon per mode [28]. In this paper, $|g_{12}^{(1)}|$ denoting $|g_{12}^{(1)}(\lambda, t_1 - t_2)|$ at $t_1 - t_2 = 0$ is used to investigate the wavelength dependence of the coherence. $|g_{12}^{(1)}|$ is a positive number that lies in the interval $[0;1]$, where the value of 1 represents perfect coherence. As shown in Fig. 8(b), the degree of the coherence is almost perfect 1 over the whole spectral range of the output SC spectrum but drops quickly and oscillating at the two sides. Consequently, the SC spectrum exhibits an excellent degree of coherence.

Moreover, Fig. 9 shows the spectrogram of the output pulse at the propagation distance of 0.1 m. One can see that the frequency components distribute monotonically across the pulse profile in the temporal domain due to the all normal flat dispersion in the fiber.

Furthermore, the SC spectra generated in the fibers with the different values of n_a are shown in Fig. 10. In order to estimate the flatness of the output spectrum, the parameter V_s is defined as the difference between the maximum and minimum values of the spectral intensities in the wavelength range of 1000 to 2600 nm. The results show that the values of V_s for the curves A, B, C, D and E are 2.13, 2.88, 3.82, 4.78, and 5.25 dB, respectively. The reason is that, when the wavelength bandwidth with the dispersion slope below $0.03 \text{ ps/nm}^2/\text{km}$ shifts toward the blue side as shown in Fig. 5(b), the spectral energy of the pump pulse can be further transferred into the higher frequency components via the effects of FWM. For the given pump pulse at the wavelength of 1550 nm, the spectral broadening on the blue side results in the decrease of the spectral intensity and, then, the degradation of the spectral flatness over the wavelength range of 1000–2600 nm.

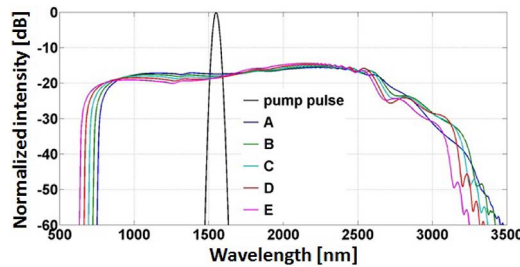


Fig. 10. SC spectra generated in the fiber with the length of 0.1 m and the spectrum of the pump pulse. The central wavelength of the pump pulse is 1550 nm with $E_0 = 25$ nJ and $T_{FWHM} = 100$ fs. The fiber parameters for the five curves are identical to those in Table 1.

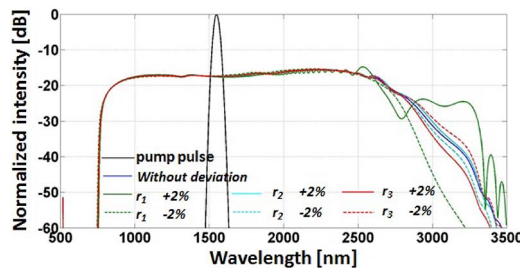


Fig. 11. SC spectra generated in the fiber with the length of 0.1 m and the spectrum of the pump pulse. The central wavelength of the pump pulse is 1550 nm with $E_0 = 25$ nJ and $T_{FWHM} = 100$ fs. The fiber parameters without the deviations are identical to those of curve A in Table 1.

Fig. 11 shows the output SC spectra when the radii r_1 , r_2 and r_3 are changed by $\pm 2\%$, respectively. The corresponding dispersion curves and fiber parameters are identical to those in Fig. 4(a). When the radii r_1 , r_2 , and r_3 increase by 2%, the values of V_s are 2.90, 2.02, and 2.38 dB. When the radii decrease by 2%, the corresponding values of V_s are 3.12, 2.24, and 2.04 dB, respectively. The results again show that when the parameters r_2 and r_3 are changed below $\pm 2\%$, the influence of the deviations on the spectral flatness is negligible. In contrast, the $\pm 2\%$ changes of the radius r_1 result in increasing the values of V_s by around 1 dB.

4. Conclusion

An approach based on the heavily Ge-doped step-index silica fiber is proposed to obtain the all-normal flat dispersion in the fiber. The heavily Ge-doped fiber with an appropriate choice of the parameters exhibits a flat normal dispersion profile in the spectral regime 1540–2600 nm. The corresponding values of the dispersion slope are between -0.0058 and 0.03 ps/nm 2 /km. Furthermore, the numerical results show that the flat-top SC spectrum ranging from 1000 to 2600 nm can be realized by launching the pump pulse with the central wavelength of 1550 nm in the fiber. The heavily Ge-doped fiber with a four-layer refractive index profile provides an easy way to obtain all-fiber coherent SC light source because of the simple fiber structure and the SC generation with the spectral width of more than one octave.

Acknowledgment

The authors would like to thank Dr. H. R. Guo for his valuable suggestions for the improvement in the program code of the GNLSE.

References

- [1] B. Povazay *et al.*, "Submicrometer axial resolution optical coherence tomography," *Opt. Lett.*, vol. 27, no. 20, pp. 1800–1802, Oct. 2002.

- [2] H. N. Paulsen, K. M. Hilligse, J. Thøgersen, S. R. Keiding, and J. J. Larsen, "Coherent anti-Stokes Raman scattering microscopy with a photonic crystal fiber based light source," *Opt. Lett.*, vol. 28, no. 13, pp. 1123–1125, Jul. 2003.
- [3] A. M. Heidt *et al.*, "High quality sub-two cycle pulses from compression of supercontinuum generated in all-normal dispersion photonic crystal fiber," *Opt. Exp.*, vol. 19, no. 15, pp. 13 873–13 879, Jul. 2011.
- [4] A. M. Heidt, "Pulse preserving flat-top supercontinuum generation in all-normal dispersion photonic crystal fibers," *J. Opt. Soc. Amer. B, Opt. Phys.*, vol. 27, no. 3, pp. 550–559, Mar. 2010.
- [5] L. E. Hooper, P. J. Mosley, A. C. Muir, W. J. Wadsworth, and J. C. Knight, "Coherent supercontinuum generation in photonic crystal fiber with all-normal group velocity dispersion," *Opt. Exp.*, vol. 19, no. 6, pp. 4902–4907, Mar. 2011.
- [6] A. Hartung, A. M. Heidt, and H. Bartelt, "Pulse-preserving broadband visible supercontinuum generation in all-normal dispersion tapered suspended-core optical fibers," *Opt. Exp.*, vol. 19, no. 13, pp. 12 275–12 283, Jun. 2011.
- [7] A. M. Heidt *et al.*, "Coherent octave spanning near-infrared and visible supercontinuum generation in all-normal dispersion photonic crystal fibers," *Opt. Exp.*, vol. 19, no. 4, pp. 3775–3787, Feb. 2011.
- [8] I. A. Sukhoivanov *et al.*, "Supercontinuum generation at 800 nm in all-normal dispersion photonic crystal fiber," *Opt. Exp.*, vol. 22, no. 24, pp. 30 234–30 250, Dec. 2014.
- [9] H. Tu *et al.*, "Scalar generalized nonlinear Schrödinger equation-quantified continuum generation in an all-normal dispersion photonic crystal fiber for broadband coherent optical sources," *Opt. Exp.*, vol. 18, no. 26, pp. 27 872–27 884, Dec. 2010.
- [10] M. Klimczak *et al.*, "Coherent supercontinuum generation up to $2.3 \mu\text{m}$ in all-solid soft-glass photonic crystal fibers with flat all-normal dispersion," *Opt. Exp.*, vol. 22, no. 15, pp. 18 824–18 832, Jul. 2014.
- [11] A. Ferrando, E. Silvestre, P. Andres, J. Miret, and M. Andres, "Designing the properties of dispersion-flattened photonic crystal fibers," *Opt. Exp.*, vol. 9, no. 13, pp. 687–697, Dec. 2001.
- [12] K. Hansen, "Dispersion flattened hybrid-core nonlinear photonic crystal fiber," *Opt. Exp.*, vol. 11, no. 13, pp. 1503–1509, Jun. 2003.
- [13] K. M. Gundu, M. Kolesik, J. V. Moloney, and K. S. Lee, "Ultra-flattened-dispersion selectively liquid-filled photonic crystal fibers," *Opt. Exp.*, vol. 14, no. 15, pp. 6870–6878, Jul. 2006.
- [14] W. Q. Zhang, H. E. Heidepriem, T. M. Monro, and V. S. Afshar, "Fabrication and supercontinuum generation in dispersion flattened bismuth microstructured optical fiber," *Opt. Exp.*, vol. 19, no. 22, pp. 21 135–21 144, Oct. 2011.
- [15] A. Bouk, A. Cucinotta, F. Poli, and S. Selleri, "Dispersion properties of square-lattice photonic crystal fibers," *Opt. Exp.*, vol. 12, no. 5, pp. 941–946, Mar. 2004.
- [16] S. M. A. Razzaq and Y. Namihira, "Tailoring dispersion and confinement losses of photonic crystal fibers using hybrid cladding," *J. Lightw. Technol.*, vol. 26, no. 13, pp. 1909–1914, Jul. 2008.
- [17] T. Martynkien, D. Pysz, R. Stępień, and R. Buczyński, "All-solid microstructured fiber with flat normal chromatic dispersion," *Opt. Lett.*, vol. 39, no. 8, pp. 2342–2345, Apr. 2014.
- [18] A. Camerlingo *et al.*, "Near-zero dispersion, highly nonlinear lead-silicate W-type fiber for applications at $1.55 \mu\text{m}$," *Opt. Exp.*, vol. 18, no. 15, pp. 15 747–15 756, Jul. 2010.
- [19] F. Poletti *et al.*, "All-solid highly nonlinear single mode fibers with a tailored dispersion profile," *Opt. Exp.*, vol. 19, no. 1, pp. 66–80, Jan. 2011.
- [20] V. M. Mashinsky *et al.*, "Germania-glass-core silica-glass-cladding modified chemical-vapor deposition optical fibers: Optical losses, photorefactivity, and Raman amplification," *Opt. Lett.*, vol. 29, no. 22, pp. 2596–2598, Nov. 2004.
- [21] Y. P. Yatsenko *et al.*, "Four-wave mixing with large Stokes shifts in heavily Ge-doped silica fibers," *Opt. Lett.*, vol. 30, no. 15, pp. 1932–1934, Aug. 2005.
- [22] O. I. Medvedkov, S. A. Vasiliev, P. I. Gnusin, and E. M. Dianov, "Photosensitivity of optical fibers with extremely high germanium concentration," *Opt. Mater. Exp.*, vol. 2, no. 11, pp. 1478–1489, Nov. 2012.
- [23] S. Sakaguchi and S. Todoroki, "Optical properties of GeO_2 glass and optical fibers," *Appl. Opt.*, vol. 36, no. 27, pp. 6809–6814, Sep. 1997.
- [24] J. W. Fleming, "Dispersion in $\text{GeO}_2\text{-SiO}_2$ glasses," *Appl. Opt.*, vol. 23, no. 24, pp. 4486–4493, Dec. 1984.
- [25] G. P. Agrawal, *Nonlinear Fiber Optics*. New York, NY, USA: Academic, 2006.
- [26] A. Boskovic, L. Gruner-Nielsen, O. A. Levring, S. V. Chernikov, and J. R. Taylor, "Direct continuous-wave measurement of n_2 in various types of telecommunication fiber at $1.55 \mu\text{m}$," *Opt. Lett.*, vol. 21, no. 24, pp. 1966–1968, Dec. 1996.
- [27] Y. Yatsenko and A. Mavritsky, "D-scan measurement of nonlinear refractive index in fibers heavily doped with GeO_2 ," *Opt. Lett.*, vol. 32, no. 22, pp. 3257–3259, Nov. 2007.
- [28] J. M. Dudley, G. Genty, and S. Coen, "Supercontinuum generation in photonic crystal fiber," *Rev. Mod. Phys.*, vol. 78, no. 4, pp. 1135–1184, Oct. 2006.
- [29] K. Rottwitt and J. H. Povlsen, "Analyzing the fundamental properties of Raman amplification in optical fibers," *J. Lightw. Technol.*, vol. 23, no. 11, pp. 3597–3605, Nov. 2005.
- [30] F. Poletti and P. Horak, "Dynamics of femtosecond supercontinuum generation in multimode fibers," *Opt. Exp.*, vol. 17, no. 8, pp. 6134–6147, Apr. 2009.